Review of Scientific Instruments

RESEARCH ARTICLE | SEPTEMBER 01 2022

Maximum power point tracking for a multi-layered piezoelectric heel charger with a levered mechanism toward impact-based energy harvesting

Rui Hua ; Sebastian Marin-Quiros ; Harsha Kalkunte Mohan; Ya Wang

Rev. Sci. Instrum. 93, 095001 (2022)
https://doi.org/10.1063/5.0091254
CHORUS

Review of Scientific Instruments ARTICLE scitation.org/journal/rsi

Maximum power point tracking for a multi-layered piezoelectric heel charger with a levered mechanism toward impact-based energy harvesting

Cite as: Rev. Sci. Instrum. 93, 095001 (2022); doi: 10.1063/5.0091254
Submitted: 13 March 2022 • Accepted: 2 August 2022 •
Published Online: 1 September 2022

Rui Hua,[1] Sebastian Marin-Quiros,[2] Harsha Kalkunte Mohan,[1] and Ya Wang[1,3,4,a)]

AFFILIATIONS

[1] J Mike Walker' 66 Department of Mechanical Engineering, Texas A&M University, 3123 TAMU, College Station, Texas 77843, USA
[2] Department of Mechanical Engineering, Stanford University, 450 Serra Mall, Stanford, California 94305, USA
[3] Department of Biomedical Engineering, Texas A&M University, 3120 TAMU, College Station, Texas 77843, USA
[4] Department of Electrical and Computer Engineering, Texas A&M University, 3128 TAMU, College Station, Texas 77843, USA

[a)] **Author to whom correspondence should be addressed:** ya.wang@tamu.edu

ABSTRACT

The piezoelectric footstep energy harvester does not always work at its maximum power point when the external load is fixed, as the optimal load changes when the walking excitation alters. Thus, the harvesting efficiency is downgraded largely in real-life scenarios compared to in-lab experiments and theoretical or numerical predictions due to the mismatch between the actual load and the optimal load. To address this issue, the concept of Maximum Power Point Tracking (MPPT) is investigated in this paper and the circuit design is implemented for a multi-layered levered piezoelectric footstep energy harvester (heel charger). The proposed event-driven MPPT circuit interface with a customized buck converter aims to maximize the power gained from daily walking using the heel charger to power a fixed load, such as smart insole or shoes. The MPPT circuit design is conceptually simulated and then tested with the heel charger to further validate if it works at its maximum power point when the frequency of the input excitation alters. Results show that the extracted power from the heel charger connected to a fixed resistance load with MPPT implementation is improved up to 300% compared to the one without MPPT implementation in simulation and up to 180% in the experiment when connected to a fixed load. The difference between simulation and experimental results is due to the optimization of using voltage sources as the heel charger and the control signals (pulse width modulation) from the microcontroller in the simulation.

I. INTRODUCTION

Over the past decade, smart shoe devices[1–3] have gained ever-increasing attention from multi-disciplinary communities and have been utilized in applications, such as activity tracking,[4–7] gait monitoring,[8–12] fitness evaluation, and human–machine interactions.[13–15] One of the key restrictions of employing smart insole or shoe devices in daily life is the significant energy limitation[16] as the frequent replacements and charging of batteries is inconvenient. To self-power smart insole or shoe devices, footstep energy is a promising, accessible, and renewable energy source.

Footsteps are a low frequency energy source with a relatively low power conversion efficiency.[17] Up to date, various designs of footstep energy harvesters[18] have been proposed, generally with one or a combination of typical transducing mechanisms, including the electromagnetic, electrostatic, triboelectric, and piezoelectric mechanisms. For instance, an electromagnetic energy harvester[19] is designed for low-frequency and irregular motions. Although this device can be excited in any direction and generate 10.4 mW at 8 Hz frequency excitation with a volume of 33.1 cm^3 from experiments, the physical volume of the device required to produce a substantial power output is too large to be reasonably equipped into a shoe. Another energy harvesting strategy[20] uses a smaller-volume electrostatic vibration energy harvesting system with a frequency up-conversion system, but the reported efficiency is between 4% and 8%, requiring over 4 min to charge a 47 uF capacitor to 3.5 V.

Because of the excellent flexibility and stretchability, the triboelectric effect is gaining attention to convert footstep energy to electricity, but the power density is small that the power generated by most of studies is only hundreds uW.[21,22] Compared to all of the above, piezoelectric transducers are more applicable to the in-shoe integration[23–26] with the advantages of high power density and different structural designs, which can be mainly classified into three types:[18] flat plate, arch, and cantilever. To name a few, Rocha *et al.*[23] have designed an energy harvesting system integrated into the shoe using parallel polyvinylidene fluoride (PVDF) piezoelectric layers. Almusallam *et al.*[25] have reported a screen-printed piezoelectric composite that can be printed on flexible substrates, such as a shoe-insole. Most of the studies[23–26] have reported encouraging results of the maximum power from their in-lab experiments: under fixed excitation levels for the purpose of characterizing the optimal load and periodical excitations.

However, in real-life scenarios, walking is not consistently periodical as we may stop, speed up, and slow down during a period. There is a mismatch between the optimal load and the actual load on the system when the walking excitation frequency alters. Because of this, the harvester does not always work at its maximum power point when the external load is fixed. Thus, the extracted energy with the optimal load reported in many in-lab experimental studies[23–26] does not always represent its real harvesting performance in real-life scenarios, where the excitation alters but the load is often fixed.

To extract more energy from piezoelectric energy harvesters and to improve the conversion efficiency, various circuit interfaces,[27] such as Synchronized Switch Harvesting on Inductor (SSHI)[28,29] and Synchronized Electric Charge Extraction (SECE),[30] are developed[31,32] and well summarized in an excellent review.[33] Even though these circuit interfaces are proven to be effective, none of them are designed for tracking the maximum power point when the excitation alters. Note that, SECE solution provides consistent power output because of its feature of load independence, but the actual power output is usually lower than the maximum power predicted by theoretical modeling or numerical simulation. To this matter, Maximum Power Point Tracking (MPPT), which has gained great successes in solar energy harvesting,[34,35] is a promising solution to be integrated with the SSHI circuit interfaces to maintain the maximum power output for the load dependent SSHI. However, up to date, there are only a few studies[36–39] working on integrating MPPT with piezoelectric energy harvesters. For instance, Kawai *et al.*[38] have designed an open-circuit MPPT controlled piezoelectric energy harvesting circuit based on SSHI to dynamically track the maximum power points when excitation alters, which used 200 Hz vibration-based excitations. To our best knowledge, low-frequency footstep energy harvesting with MPPT implementation is not well explored. Besides MPPT, a most recent study[40] uses long short-term memory (LSTM) network-based classifiers to accurately detect walking and then collect footstep energy through piezoelectronics-based device. Such a gait-driven method shows up to 127% more energy collected through recognizing gait. However, LSTM learning model needs to be trained with quite an amount of data and is not robust when applied to different users, and thus the improvement will be user dependent. Moreover, it is very power consuming to be implemented in a wearable device with energy limitations.

Thus, this paper aims to prove the circuit implementation of MPPT as the interface to a footstep energy harvester can improve the harvesting efficiency under real-life scenarios. A threshold-based event-driven MPPT circuit interface is proposed for a customized multi-layer levered piezoelectric footstep energy harvester (heel charger with SSHI circuit interface),[26] positioned at the heel area. The simple MPPT circuit interface, including a buck converter design with the open-circuit MPPT method, is designed and implemented to gain the maximum energy from the heel charger to power a fixed load: smart insole (MONI),[41] which is designed for gait monitoring and activity recognition. The proposed method provides a solution to decreasing the mismatch between the optimal load in lab tests and the actual load in real-life scenarios and bridge the gap of applying MPPT to footstep energy harvesting. We hope our proposed method will further promote the lab-tested footstep energy harvesters from vibration-based to real-life applications of the impact-based energy harvesting.

II. DESIGN OVERVIEW

A. Case study and logic of event-driven MPPT

Figure 1 shows the DC voltage output from the heel charger with a full-bridge AC–DC rectifier in a real walking case covering most of the daily walking conditions. It shows phases of starting from standby, slow walking, speeding up, stopping for seconds, speeding up again, stopping for a few seconds and speeding up and slowing down. Clearly, the maximum power point of the heel charger changes every time when the walking excitation changes. After MPPT applied, the heel charger is ensured to work around its maximum power point and the harvesting efficiency is largely increased compared to the heal charger without MPPT implementation.

However, a periodical MPPT implementation may waste power as MPPT operates even when it is not necessary. Thus, an event-driven MPPT is proposed to make sure most of the MPPT operations are triggered only when needed. It is triggered by events: (1) a pre-defined voltage threshold Th and (2) an increasing gap ΔV and an increasing gap threshold ΔTh. The logic of the event-driven MPPT is detailed in Fig. 2.

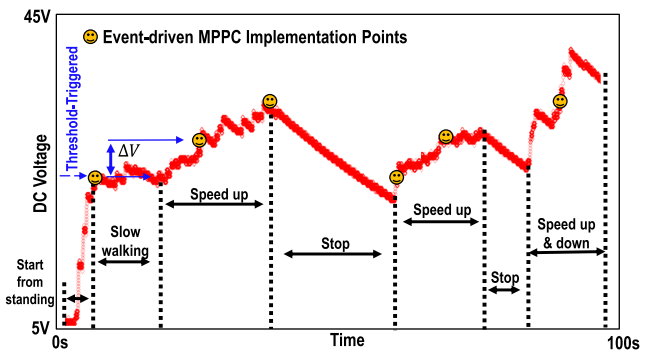

FIG. 1. Proposed event-driven MPPT applied to heel charger voltage output from real-case walking.

Algorithm: Event-driven MPPT

1. $V \leftarrow$ Voltage from heel charger
2. $Th \leftarrow$ Voltage threshold to trigger MPPT
3. $\Delta V \leftarrow$ Voltage change to trigger MPPT
4. $\Delta Th \leftarrow$ Voltage change threshold
5. while True:
6. if V $\geq Th$ then
7. $\Delta V = V - V_{temp}$
8. if $\Delta V \geq \Delta Th > 0$ then
9. $V_{temp} = V$
10. MPPT triggered
11. if $\Delta V < -\Delta Th < 0$ then
12. $V_{temp} = V$

FIG. 2. Logic of event-driven MPPT.

When the output voltage of the heel charger reaches the predefined voltage threshold, the increasing gap is calculated; when the increasing gap is larger than the increasing gap threshold, the MPPT is triggered. V_{temp} is an internal variable to keep the voltage of the previous point of MPPT implementation or the output voltage of the heel charger when it drops more significantly than the increasing gap threshold. The MPPT is only triggered when the user keeps speeding up, speeds up after stopping or slowing down. Compared to periodical MPPT, the event-driven MPPT gains the maximum energy harvesting efficiency by not being triggered in the unnecessary conditions of the user stopping or slowing down when the heel charger tends to stop harvesting energy. When MPPT is not triggered, the harvesting energy keeps flowing to the buck converter and the load under the last time MPPT adjustment. The system works close to the maximum power point.

B. Hardware design

Figure 3 shows the block view of the proposed hardware design, including the heel charger, the AC–DC circuit interface (converting AC to DC voltage), the MPPT blocks, a super capacitor to store energy, and a voltage regulator to continuously power MPPT implementation and the fixed load including accelerometers in the smart insole. The AC–DC circuit interface is an SSHI circuit followed by a full bridge rectifier. The MPPT blocks include a switch, a customized buck converter and a microcontroller (MCU) to run the MPPT algorithm, which is an open-circuit MPPT method to be detailed in Sec. IV A. The switch keeps switching on and off for the implementation of the open-circuit MPPT. The buck converter is customized with only a few electric components to step down the voltage, increase the output current, and optimize the load resistance to the optimal load. The MCU provides control signals to the switch to sample open-circuit voltage and close-circuit voltage, and control signals to the buck converter to adjust the actual load close to the optimal load of the heel charger.

III. PIEZOELECTRIC FOOTSTEP ENERGY HARVESTER

A. Heel charger design

Here, we use a two-layer piezoelectric heel charger[26] developed by our group. The prototype in the top view is as shown in Fig. 4(a). Figure 4(b) is the view of rotating Fig. 4(a) at the lateral axis. From experiments, we record the DC voltage at the maximum power points for various excitations (frequency between 1 and 2.3 Hz, force from ~100 to ~200 N) and the open-circuit voltage V_{OC}, which is the voltage output of the heel charger when no load is connected. Figure 4(c) shows a linear fitting curve between V_{OC} and the close-circuit voltage at the maximum power point V_{MPP}. The slope of the curve is the experimental K value for the heel charger: K = 0.4861, which is one of the essentials in the open-circuit MPPT method. Our experimental results are consistent to the existing studies,[36–39] where the K value of the piezoelectric energy harvester is around 0.5.

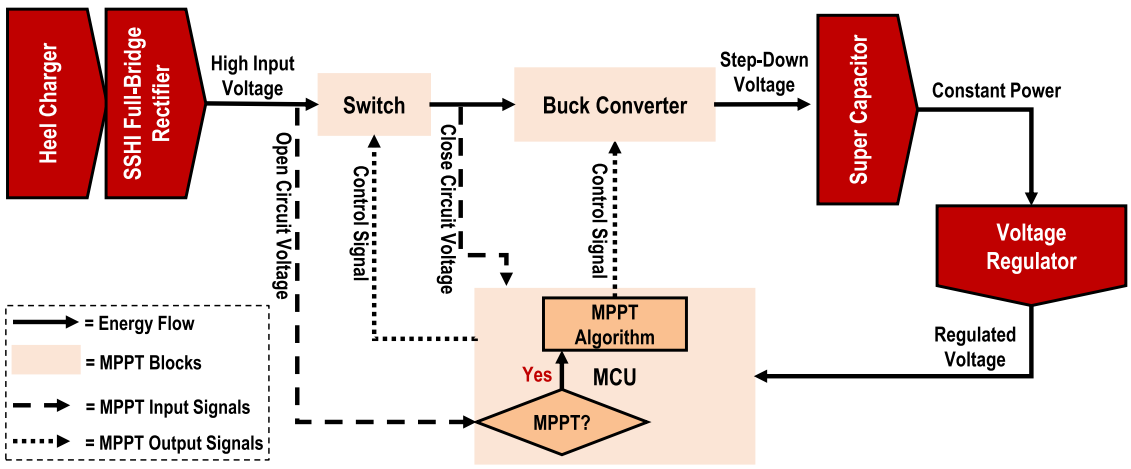

FIG. 3. System design in block view.

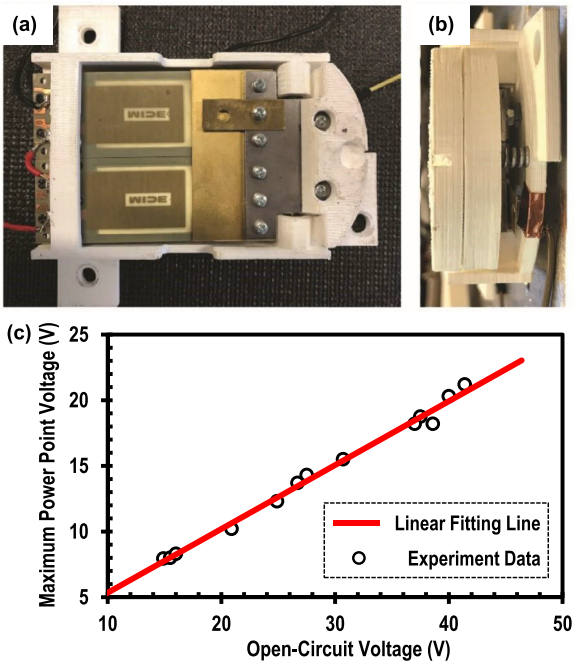

FIG. 4. (a) Top view of the heel charger; (b) side vies; and (c) linear fitting coefficient: *K* value of heel charger from experimental results.

B. Performance discussion

As the human normal walking frequency is between 1.5 and 2.3 Hz,[42] the heel charger with the AC–DC circuit interface has been tested with the shaker in various frequencies from 1.5, 2, 2.3, and 3 Hz with forces of 220 N in sine-wave excitations from our previous experiments of characterization.[26] Figures 5(a)–5(c) show the test results of power, output DC voltage, and current when sweeping load resistances from several ohm to 1M ohm. The DC power output of the heel charger varies from less than 1 mW to up to 7 mW when connecting to different load resistances. Thus, the mismatch of load resistance to the source internal resistance degrades the harvesting energy several to hundreds of times. Table I summarizes the key property parameters of the heel charger with the circuit interface, which are the referenced design parameters for the buck converter design in Sec. IV B. If smaller force is applied, the ranges of these parameters are within the ranges listed in Table I.

TABLE I. Key parameters of heel charger.

Heel charger	
Input voltage range	[0, 50 V]
Input current range	[0, 300 uA]
Internal resistance R_{HL}	[0, 1M] ohm
Optimal load resistance R_{opt}	[180k, 250k] ohm

IV. OPEN-CIRCUIT MPPT IMPLEMENTATION

A. Open-circuit MPPT method

There are a lot of MPPT methods[34,35,43] developed and proven to be useful in solar energy harvesting. Here, we have chosen the open-circuit MPPT method[44] as it is fast and easily implemented with low power consumption in comparison with other MPPT methods, such as hill climbing,[45] perturb and observe,[46] or machine learning with high computational complexity.[47] The open-circuit MPPT method is based on the relation between the open-circuit voltage V_{OC} and the close-circuit voltage at the maximum power point V_{MPP} when the heel charger is connected to its optimal load

$$V_{MPP} = K \cdot V_{OC}, \tag{1}$$

where K is a constant. By sampling the V_{OC} in real time, V_{MPP} can be calculated as our target of the closed-circuit voltage. Further sampling the closed-circuit voltage and adjusting the load value, it matches the closed-circuit voltage to the V_{MPP} when the load matches to the optimal load to the heel charger. The working principle of adjusting the load value is stated in the next sub-session of 4.2.

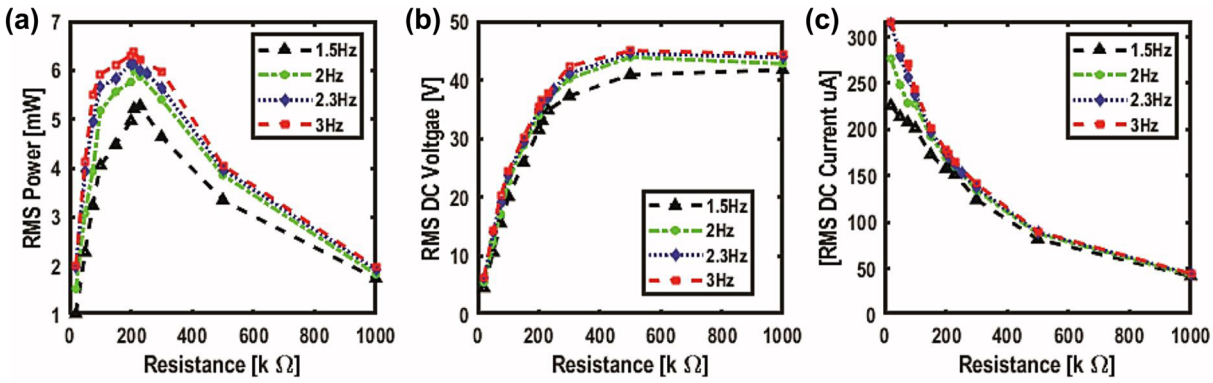

FIG. 5. Test results of heel charger properties: (a) RMS power, (b) output DC voltage, and (c) current when sweeping load resistances from several ohm to 1M ohm.

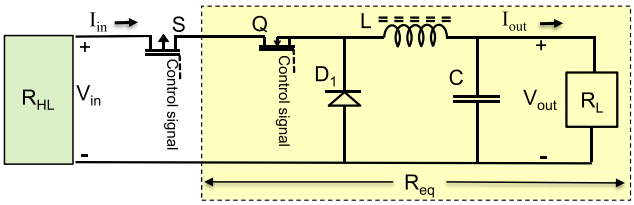

FIG. 6. Open-circuit MPPT with buck converter implementation.

TABLE II. Key design parameters of the buck converter.

Parameters	Values
Output voltage range	[0, 15 V]
Output current range	[0, 700 μA]
Equivalent load resistance R_{eq}	[200k, 250k] ohm
Control signal duty cycle D	[0, 1]
Control signal frequency f	~Hundred kHz
L max voltage	50 V
C max voltage	45 V
S max voltage	100 V
Q max voltage	100 V
D_1 max voltage	50 V

B. Buck converter design

The buck converter is customized for the heel charger to step the output voltage down, increase the output current, and match the optimal load for maximum energy harvesting. Figure 6 is a circuit-level view of the buck converter. The buck converter includes a transistor Q, a diode D_1, an inductor L, and an output capacitor C. R_{HL} is the equivalent resistance of the heel charger and the AC–DC circuit interface; R_L is the actual fixed load; and R_{eq} is the equivalent resistance of the yellow shaded area, including the buck converter and R_L. When the switch S is on, the resistance of S can be ignored.

The principle of the buck converter is that Q and D_1 keep switching on and off alternatively at a high frequency with a Pulse Width Modulation (PWM) control signal of a duty cycle D to Q. For the buck converter, the input/output voltage and current are defined in Fig. 6 as V_{in}, I_{in}, V_{out}, and I_{out}. We have

$$V_{out} = D \cdot V_{in} \quad \text{and} \quad I_{in} = D \cdot I_{out}. \tag{2}$$

Assuming that the buck converter is energy lossless, the input power to the buck converter is equal to the output power: $V_{in}I_{in} = V_{out}I_{out}$. We have

$$R_{eq} = \frac{R_L}{D^2}. \tag{3}$$

Thus, the buck converter up-converts the load resistance R_L to match the optimal load to the source, depending on the duty cycle of the control signal to Q. Table II lists the key design parameters of the buck converter when choosing the components with considerations of the properties of the heel charger.

C. Working principles—Circuit-level

To detailed explain the system design block view in Fig. 3, Fig. 7 is a circuit-level implementation of the hardware design. Three blocks are defined: energy source block, including the heel charger with SSHI and a full-bridge rectifier; MPPT block, including the buck converter and other components of implementing open-circuit MPPT; and load block, including a block-diode, a super capacitor C_s, and a voltage regulator to ensure the energy will not flow back and the final output voltage is stabilized at 3.3 V.

Figure 8 shows the working principles of the proposed MPPT method in the circuit-level of the MPPT block. The conductive parts are in red, while the non-functional parts are in black. There are two phases when implementing MPPT:

- Figure 8(a) Phase 1: Sampling open-circuit voltage by turning off switch S. This is the start of event-driven MPPT implementation, triggered by the events defined in Sec. II A. Phase 1 only lasts for a few milliseconds as there is no energy in Phase 1.
- Figure 8(b) Phase 2: Sampling close-circuit voltage by turning on switch S. Once the open-circuit voltage is sampled, the target voltage at the maximum power point can be calculated with Eq. (1). By sampling close-circuit voltage, the duty cycle of the PWM control signal to Q is being adjusted to minimize the gap between the target voltage and the close-circuit voltage. Repeat Phase 2 until the gap is approaching 0.
- Figures 8(c) and 8(d) Phase 2.1 and Phase 2.2 are the sub-phases in Phase 2 of how the buck converter works in the

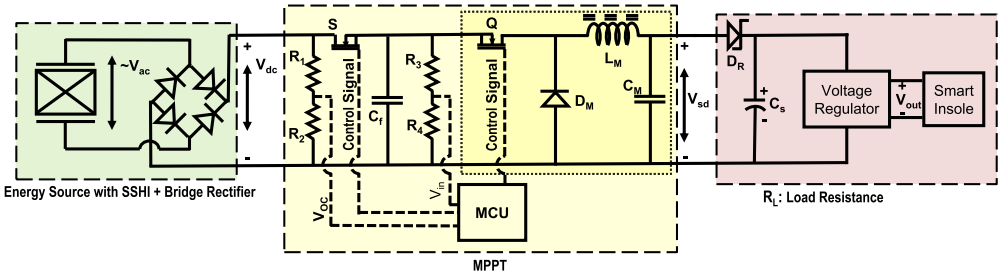

FIG. 7. The proposed MPPT circuit interface design in circuit-level view.

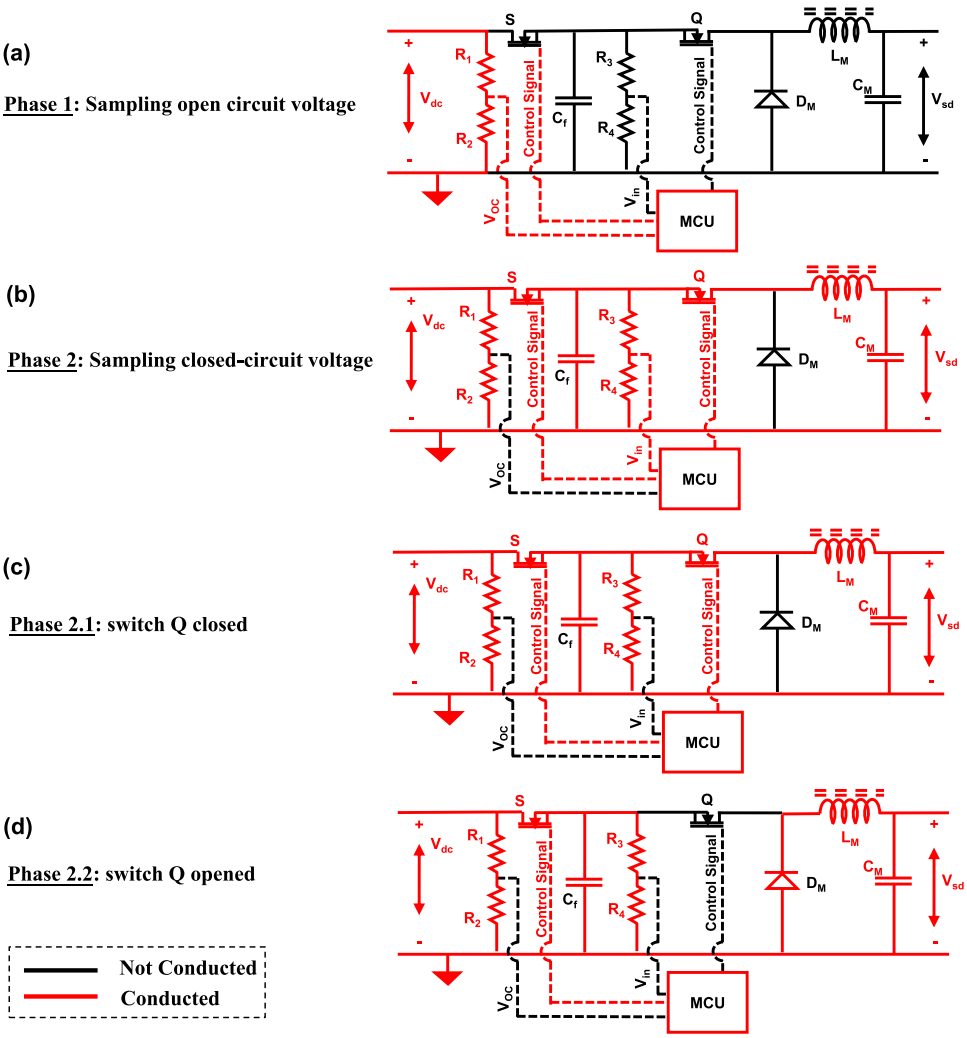

FIG. 8. Working principles of the MPPT: (a) phase 1; (b) phase 2; (c) phase 2.1; and (d) phase 2.2.

circuit-level: Turning on and off switch Q at hundreds kHz. Here, R_{eq} is adjusted accordingly as shown in Eq. (3).

Based on the component selection principles in Table II, we select the MPPT block components and detailed the models and values in Table III for simulation and experiments.

V. SIMULATION RESULTS

To conceptually prove our proposed method in the circuit-level, we build up the circuit-level simulation of the MPPT blocks with periodical MPPT implementation in LTspice XVII (developed by Linear Technology and Analog Devices) with the spice models of each component (except the MCU) in Table III. To simulate the DC output of the energy source block, we use a DC voltage source with an internal resistance that provides a V_{oc} between 10 and 40 V as the same range as in Fig. 5. To simulate the PWM output from the

TABLE III. Components for the MPPT block in Fig. 7.

Component	Model/Value
S, Q	Si7113DN
D_M	DAP222M
L_M	0.1 H
C_f	0.1 μF
C_M	100 μF
D_R	1N4003
R_1	20M ohm
R_2	1.7M ohm
R_3	20M ohm
R_4	1.7M ohm
MCU	MSP430
Full-bridge rectifier	1N4007 $*$ 4
Voltage regulator	AP7380

TABLE IV. MPPT block simulation results.

Simulation case (Hz)	Open circuit voltage V_{oc} (V)	Closed circuit voltage V_{in} (V)	Target close-circuit voltage V_{mpp} (V)	Error %	Output power improvement %
Case 1: 1	22	11	10.7	2.8	309
Case 2: 1.5	32	16	15.6	2.6	227
Case 3: 2	41	20.9	19.9	5.3	206

MCU, we use pulse wave voltage generators to produce the PWM control signals. We run the simulation to record the buck converter output V_{sd}, the buck converter output current I_{sd}, the V_{oc}, and the V_{in} with and without the implementation of MPPT.

We simulate a few cases, V_{oc} = 22, 32 and 41 V, corresponding to excitation frequency of around 1, 1.5, and 2 Hz with a large force applied at about 220 N from our previous experiments in Fig. 5. The results are shown in Table IV. The target close-circuit voltage at the maximum power point V_{mpp} is calculated with Eq. (2). The frequency of the control signal (PWM) to Q is 100 kHz.

Error is calculated as

$$Error = \frac{V_{in} - V_{mpp}}{V_{mpp}} \times 100\%. \quad (4)$$

We also run simulations without MPPT implementation as comparisons. The output power without MPPT is simulated by changing a load resistance (30k ohm larger as the benchmarks) without the MPPT implementation, where the MPPT block is functionalized the same as a buck converter without MPPT functionality. The improvement depends on the resistance load change of how much the actual load varies from optimal load. The output power improvements are summarized in the last column in Table IV.

The simulation results of the V_{oc}, V_{in}, and buck converter output voltage V_{sd} with the control signals to switch S and Q for simulation case 3 are shown in Figs. 9(a)–9(e). When the state is steady, the V_{in} is around half of the V_{oc} from the relation in Eq. (1), which indicates the MPPT works.

VI. EXPERIMENT RESULTS AND DISCUSSION

A. Experiment and results

The experiment has been done with the heel charger at different frequencies from 1 to 2 Hz of a small force excitation (~30 N) with the shaker to prove the proposed hardware design and MPPT works. As the experiment has been set up with the shaker for fixed excitation cases, we apply periodical MPPT to each case. Figure 10 shows the experiment setup. Instead of using the smart insole prototype as shown in the bottom left of Fig. 10, we use the circuit breakdown of the smart insole in the experiment for easy operations, but it is with the same load value as the smart insole. We use the waveform generation function of the oscilloscope as the sine-wave excitation to simulate footsteps. A power amplifier is used to amplify the power of the sine-wave excitation to drive the shaker. The heel charger is fixed on the metal support shelves attached to the shaker, connected to the circuit interface of SSHI and full bridge rectifier to produce DC voltage outputs. The MPPT block (excluding the MCU) is designed as a piece of the printed circuit board. All the waveform results are captured by the oscilloscope. Note that, as the instant power generated by the heel charger is relatively unstable to power the smart insole electronics, we use a battery to power the smart insole MCU (also runs the MPPT) in the experiment for easily debugging and monitoring the MPPT. The feasibility of how to implement the heel charger with the MPPT in real-life cases is analyzed in the section of discussion.

Table V summarizes the five cases that we perform in the experiment. The five cases cover excitations of various frequencies at a

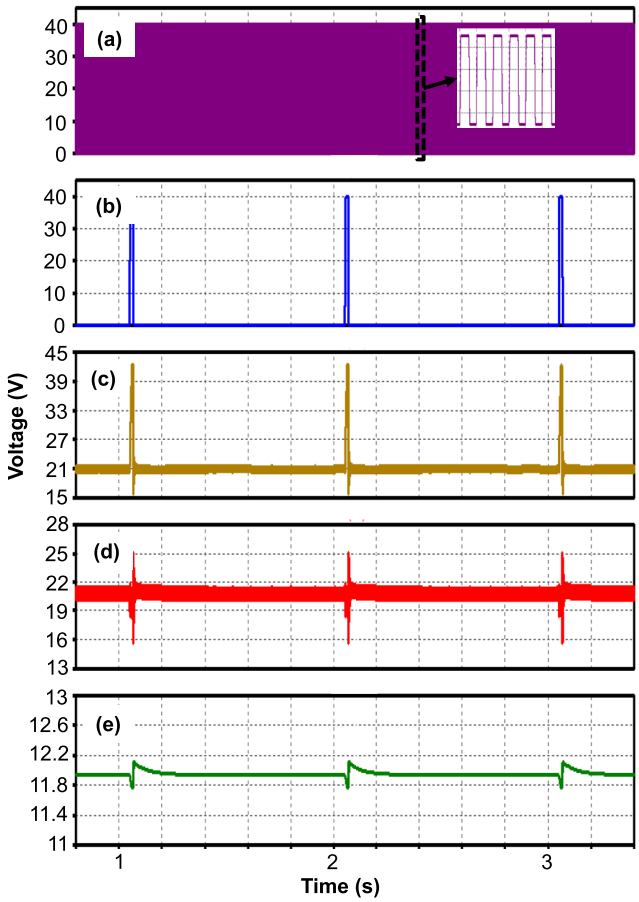

FIG. 9. Waveforms of simulation results of simulation case 3. (a) The waveforms are control signal to Q, (b) control signal to S, (c) V_{OC}, (d) V_{in}, and (e) V_{sd}. As the control signal to Q is 100 kHz frequency, an enlarged view of the control signal to Q is added to the top right of (a).

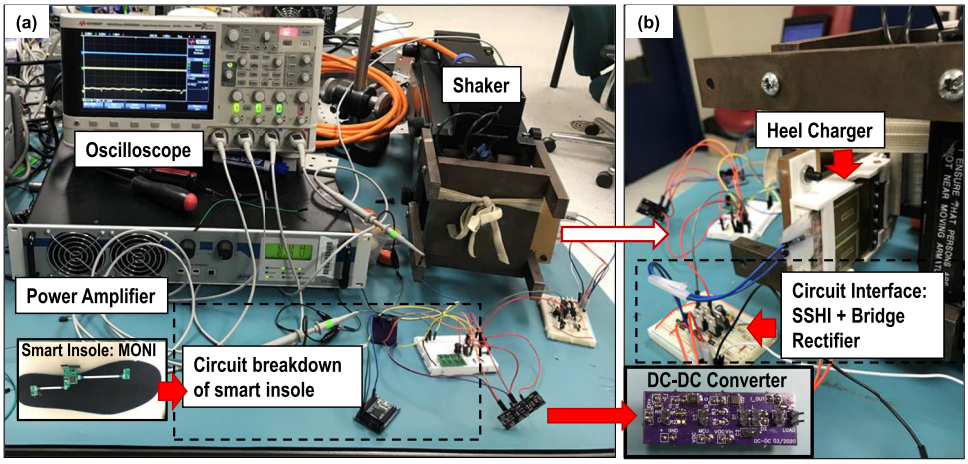

FIG. 10. Experiment setup: (a) front view and (b) side view (showing where the heel charger is mounted).

small force (~30 N). Following the open-circuit method theory and the K value of the heel charger from Eq. (1), the errors of MPPT are below 2% for each case by Eq. (4). To show the improvements of MPPT implementation, we also do experiments without the hardware of the MPPT blocks by directly connecting the load to the DC output of the circuit interface. The output power (power delivered to the load) improvement is summarized in the last column of Table V. Figure 11 details the experimental results in waveforms of case 5 with the PWM control signal. From the top to the bottom, the waveforms are control signal to Q, control signal to S, V_{OC}, V_{in}, and V_{sd}.

B. Results and discussion

We conceptually prove the MPPT circuit interface design in simulation based on our results of the heel charger properties from the previous experiments. The simulation results show improvements from 200% to 300%. In experiments, we test the hardware with excitations at 30 N and of various frequencies provided by the shaker. Experimental results show improvements from 150% to 180% for excitations at various frequencies. The difference between simulation and experimental results is mainly due to two reasons. First, a DC voltage source is used in simulation to simulate the output from the energy source block, including the heel charger with SSHI and a full-bridge rectifier, and second, the PWM voltage generators are used in simulation to represent the PWM outputs as the control signals that are from the microcontroller in experiments.

The following discussion is focused on the feasibility of applying the proposed method to real-life scenarios based on energy estimations, aiming to provide an insight into relations between self-charging and energy consumption of the smart insole as the assessment of self-powering. To estimate the self-power ability, we modify and simplify the smart insole design from our previous work[41] by reducing the working modes to sleep mode, active mode, and MPPT mode and setting up the insole to wake up every 10 s and acquire acceleration data in 1.61 s as shown in Fig. 12. In the sleep mode, the MCU is in the sleep mode with the control signal to switch Q (5.65 μW) on and the accelerometer is also in the sleep mode (1.8 μW). The energy keeps flowing from the heel charger to the energy storage, which is a super capacitor, without MPPT adjustment. If the event-driven MPPT is triggered, it enters the MPPT mode where the proposed open-circuit MPPT runs. Here, the MCU becomes active where it consumes 4170.7 μW, and the accelerometer remains sleeping. The MPPT mode can be further partitioned into three sub-modes: sampling V_{OC}, sampling V_{in} and comparing to V_{mpp}, and adjusting the duty cycle of the control signal to Q if the Vin does not match V_{mpp}. When the insole enters the active mode, the MCU and the accelerometer becomes active where the MCU consumes 4170.7 μW and the accelerometer consumes 20 μW. The power breakdown is shown in Table VI. To estimate the average power consumption, we assume that the MPPT mode is implemented periodically every 10 s and lasts 1.5 s (10 duty cycle adjustments in one MPPT implementation and every adjustment

TABLE V. MPPT experiment results.

Experimental cases (Hz)	Open circuit voltage V_{oc} (V)	Closed circuit voltage V_{in} (V)	Target close-circuit voltage V_{mpp} (V)	Error %	Output power improvement %
Case 1: 1	4.37	2.26	2.12	1.51	174
Case 2: 1.3	4.70	2.35	2.28	0.68	165
Case 3: 1.5	5.00	2.44	2.43	0.09	170
Case 4: 1.7	5.10	2.56	2.48	0.77	169
Case 5: 2	5.18	2.62	2.52	0.96	156

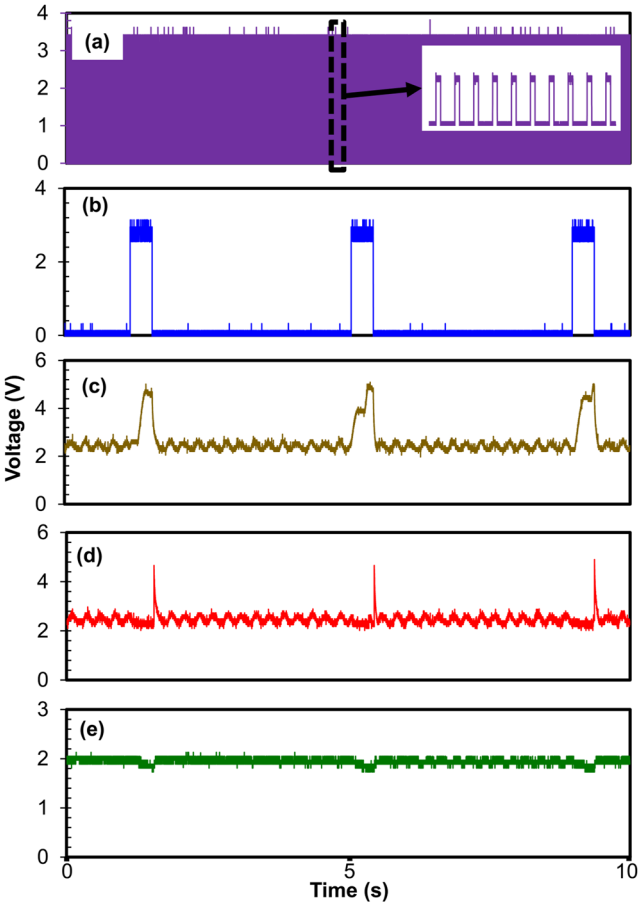

FIG. 11. Waveforms of experiment results of case 5. (a) The waveforms are control signal to Q, (b) control signal to S, (c) V_{OC}, (d) V_{in}, and (e) V_{sd}. As the control signal to Q is 100 kHz frequency, an enlarged view of the control signal to Q is added to the top right of (a).

lasts 150 ms). In such a case, the average power consumption of the smart insole is 998 μW. If a super capacitor (10 mF, 5.5 V) is used as the energy storage and it is fully charged, the energy from the super capacitor can power the smart insole 151.55 s. If the heel charger can work at its maximum power point (DC power of around 6 mW), the supercapacitor can be fully charged if the user walks 25 s. If the proposed DC–DC converter only has a conversion efficiency of 50%, the user needs to walk 50 s.

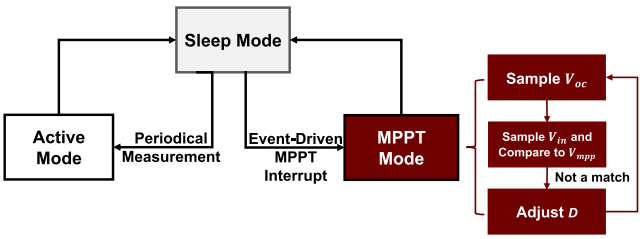

FIG. 12. Flowchart of the working mode for smart insole.

TABLE VI. Power consumption breakdown at each mode in a periodical measurement setup for smart insole and a periodical MPPT implementation.

Mode	Power (μW)	Period (s)	MCU state	Accelerometer state
Sleep mode	7.5	10	Sleep	Sleep
Active mode	4190.7	1.61	Active	Active
MPPT mode	4172.5	1.5	Active	Sleep

However, without MPPT, the worst case would be that the heel charger cannot provide any power to the smart insole when the mismatch of the equivalent load value of MONI and the optimal load value to the heel charger is large enough. Compared to the periodical implementation, the implementation of the event-driven MPPT further reduces the power consumption of the smart insole as the MPPT is only triggered when necessary as described in Sec. II A.

This paper aims to prove the feasibility of implementing the MPPT to low frequency footstep energy harvesters for real-life applications by designing an event-driven MPPT circuit interface to a piezoelectric footstep energy harvester (heel charger). Both simulation and experimental results, in addition to the self-power capability assessment, have proven the effectiveness of the proposed method. This event-driven MPPT heel charger can be integrated with smart insoles for health monitoring, and thus the event-driven MPPT can be validated and qualified of how much more power can be saved for real life scenarios. To further improve the harvesting efficiency, circuit design can be further optimized to provide a sustainable self-powering solution.

VII. CONCLUSION

Aiming to extract the maximum energy from the heel charger and bridge the gap of applying MPPT to low frequency footstep energy harvesting, we propose an event-driven MPPT circuit interface to extract the maximum energy from the heel charger and deliver to a fixed load of the smart insole with a simple customized buck converter design for real-life uses. The proposed method provides a solution to decreasing the gap between the optimal load and the actual load and it provides insights into possibilities to implement lab-tested footstep energy harvesters to real-life uses, from periodical vibration-based to impact-based energy harvesting. Our future work will address the real-life challenge: integrating the event-driven MPPT with the heel charger and the smart insole, as well as quantifying the energy harvesting performance in real life scenarios.

ACKNOWLEDGMENTS

The authors acknowledge the support of the U.S. Department of Energy ARPA-E under Grant No. DE-AR0000945.

AUTHOR DECLARATIONS

Conflict of Interest

The authors have no conflicts to disclose.

DATA AVAILABILITY

The data that support the findings of this study are available within the article or from the corresponding author upon reasonable request.

REFERENCES

[1] A. Libanori, G. Chen, X. Zhao, Y. Zhou, and J. Chen, Nat. Electron. **5**, 142 (2022).
[2] G. Chen, X. Xiao, X. Zhao, T. Tat, M. Bick, and J. Chen, Chem. Rev. **122**, 3259 (2021).
[3] I. Almuteb, R. Hua, and Y. Wang, Smart Health **25**, 100301 (2022).
[4] N. Hegde, M. Bries, T. Swibas, E. Melanson, and E. Sazonov, IEEE J. Biomed. Health Inf. **22**, 979 (2017).
[5] R. Hua and Y. Wang, in *Proceedings of 2019 IEEE Healthcare Innovations and Point of Care Technologies, (HI-POCT)* (IEEE, 2019).
[6] F. Lin, A. Wang, L. Cavuoto, and W. Xu, IEEE J. Biomed. Health Inf. **21**, 682 (2016).
[7] D. Chen, Y. Cai, X. Qian, R. Ansari, W. Xu, K.-C. Chu, and M.-C. Huang, IEEE Internet Things J. **6**, 7253 (2019).
[8] A. M. Howell, T. Kobayashi, H. A. Hayes, K. B. Foreman, and S. J. M. Bamberg, IEEE Trans. Biomed. Eng. **60**, 3284 (2013).
[9] Z. Yang, C. Song, F. Lin, J. Langan, and W. Xu, IEEE Internet Things J. **6**, 1298 (2018).
[10] Y. Charlon, A. Piau, D. Brulin, and E. Campo, Wireless Sens. Network **11**, 67 (2019).
[11] R. Das and N. Kumar, J. Med. Eng. Technol. **39**, 75 (2015).
[12] F. Martínez-Martí, M. S. Martínez-García, S. G. García-Díaz, J. García-Jiménez, A. J. Palma, and M. A. Carvajal, Australas. Phys. Eng. Sci. Med. **37**, 25 (2014).
[13] S. I. Lee, E. Park, A. Huang, B. Mortazavi, J. H. Garst, N. Jahanforouz, M. Espinal, T. Siero, S. Pollack, and M. Afridi, Med. Eng. Phys. **38**, 442 (2016).
[14] M. J. Domínguez-Morales, F. Luna-Perejón, L. Miró-Amarante, M. Hernández-Velázquez, and J. L. Sevillano-Ramos, Appl. Sci. **9**, 3970 (2019).
[15] G. Rescio, A. Leone, L. Francioso, and P. Siciliano, *Proceedings of Multidisciplinary Digital* (Publishing Institute Proceedings, 2018).
[16] A. S. Khan and F. U. Khan, Int. J. Energy Res. **46**, 2277 (2021).
[17] E. M. Nia, N. A. W. A. Zawawi, and B. S. M. Singh, in *Proceedings of IOP Conference Series: Materials Science and Engineering* (IOP Publishing, 2017).
[18] Y. Xin, X. Li, H. Tian, C. Guo, C. Qian, S. Wang, and C. Wang, Ferroelectrics **493**, 12 (2016).
[19] C. H. Huicong Liu, J. Lin, Y. Li, Q. Shi, T. Chen, L. Sun, and C. Lee, Appl. Phys. Lett. **113**, 203901 (2018).
[20] Y. Lu, F. Cottone, S. Boisseau, F. Marty, D. Galayko, and P. Basset, Appl. Phys. Lett. **107**, 253902 (2015).
[21] Y. Zou, A. Libanori, J. Xu, A. Nashalian, and J. Chen, Research **2020**, 1.
[22] Y. Zou, V. Raveendran, and J. Chen, Nano Energy **77**, 105303 (2020).
[23] J. G. Rocha, L. M. Goncalves, P. F. Rocha, M. P. Silva, and S. Lanceros-Mendez, IEEE Trans. Ind. Electron. **57**, 813 (2010).
[24] Y. Wang, W. Chen, and P. Guzman, J. Intell. Mater. Syst. Struct. **27**, 2324 (2016).
[25] A. Almusallam, R. N. Torah, D. Zhu, M. J. Tudor, and S. P. Beeby, J. Phys.: Conf. Ser. **476**(1), 012108 (2013).
[26] R. Hua, H. Liu, H. Yang, Y. Wang, and J. Ferrante, Appl. Phys. Lett. **113**, 053902 (2018).
[27] E. Lefeuvre, A. Badel, C. Richard, L. Petit, and D. Guyomar, Sens. Actuators, A **126**, 405 (2006).
[28] J. Liang and W.-H. Liao, IEEE Trans. Ind. Electron. **59**, 1950 (2011).
[29] D. Guyomar, A. Badel, E. Lefeuvre, and C. Richard, IEEE Trans. Ultrason., Ferroelectr., Freq. Control **52**, 584 (2005).
[30] E. Lefeuvre, A. Badel, C. Richard, and D. Guyomar, J. Intell. Mater. Syst. Struct. **16**, 865 (2005).
[31] J. Qiu, H. Jiang, H. Ji, and K. Zhu, Front. Mech. Eng. China **4**, 153 (2009).
[32] H. Liu, R. Hua, Y. Lu, Y. Wang, E. Salman, and J. Liang, J. Intell. Mater. Syst. Struct. **30**, 813 (2019).
[33] A. Brenes, A. Morel, J. Juillard, E. Lefeuvre, and A. Badel, Smart Mater. Struct. **29**, 033001 (2020).
[34] Z. Salam, J. Ahmed, and B. S. Merugu, Appl. Energy **107**, 135 (2013).
[35] A. Mohapatra, B. Nayak, P. Das, and K. B. Mohanty, Renewable Sustainable Energy Rev. **80**, 854 (2017).
[36] N. Kong and D. S. Ha, IEEE Trans. Power Electron. **27**, 2298 (2011).
[37] S. Bandyopadhyay and A. P. Chandrakasan, IEEE J. Solid-State Circuits **47**, 2199 (2012).
[38] N. Kawai, Y. Kushino, and H. Koizumi, in *Proceedings of IECON 2015-41st Annual Conference of the IEEE Industrial Electronics Society* (IEEE, 2015).
[39] M. Shim, J. Kim, J. Jeong, S. Park, and C. Kim, IEEE J. Solid-State Circuits **50**, 2367 (2015).
[40] D. Ma, G. Lan, W. Xu, M. Hassan, and W. Hu, IEEE Trans. Mobile Comput. **17**, 1353 (2020).
[41] R. Hua and Y. Wang, IEEE Sensors J. **19**, 6410 (2019).
[42] T. Ji and A. Pachi, Struct. Eng. **84**, 36 (2005).
[43] N. Karami, N. Moubayed, and R. Outbib, Renewable Sustainable Energy Rev. **68**, 1 (2017).
[44] A. Montecucco and A. R. Knox, IEEE Trans. Power Electron. **30**, 828 (2014).
[45] F. Liu, Y. Kang, Y. Zhang, and S. Duan, in *Proceedings of 2008 3rd IEEE Conference on Industrial Electronics and Applications* (IEEE, 2003).
[46] J. Ahmed and Z. Salam, Appl. Energy **150**, 97 (2015).
[47] A. Chaouachi, R. M. Kamel, and K. Nagasaka, Solar Energy **84**, 2219 (2010).